XLVI CILAMCE
VITÓRIA - ES - BRAZIL - 2025
XLVI IBERO-LATIN AMERICAN CONGRESS ON COMPUTATIONAL METHODS IN ENGENEERING

# Numerical Study of Blood Flow and Anisotropic Drug Diffusion in Arterial Tissue with Stents

Gabriel Mattos[1], Bernardo Coelho[2], Iury Igreja[1,2]

[1]*Department of Computer Science, Federal University of Juiz de Fora*
*Campus Universitário, Rua José Lourenço Kelmer, s/n - São Pedro, Juiz de Fora, 36036-900, Minas Gerais, Brazil*
*gabriel.mattos@estudante.ufjf.br*
[2]*Graduate Program in Computational Modeling, Federal University of Juiz de Fora*
*Campus Universitário, Rua José Lourenço Kelmer, s/n - São Pedro, Juiz de Fora, 36036-900, Minas Gerais, Brazil*
*bernardo.coelho@estudante.ufjf.br, iury.igreja@ufjf.br*

**Abstract.** Drug-eluting stents effectiveness depends on the interaction between blood flow in the arterial lumen and drug transport into adjacent tissue, which can be represented as a porous medium dominated by diffusive mechanisms that play a central role in the absorption and distribution of active compounds. Traditional models often assume Newtonian blood flow and isotropic tissue diffusion, simplifications that may compromise accuracy, especially in small-diameter arteries where non-Newtonian effects and diffusion anisotropy are significant. Comprehensive frameworks incorporating these aspects remain scarce and lack robust numerical validation. In this work, a unified computational model coupling fluid flow and drug transport in stented arteries is proposed, using Navier-Stokes equations for lumen and the Brinkman equations for porous tissue. Advection–diffusion equations govern drug transport in the lumen, while tissue transport is described by a modified diffusion equation incorporating an anisotropic diffusivity tensor. Stabilized finite element methods based on SUPG and PSPG formulations are employed to solve the coupled system, ensuring accuracy in convection-dominated regimes. The methodology is validated against benchmark literature data. The proposed model examines how blood rheology, numerical stabilization, and tissue anisotropy influence drug distribution, and compares the effects of varying stent geometries on flow patterns and drug penetration.

**Keywords:** Porous Medium, Stabilized Finite Elements, Pharmacological Stents, Anisotropic Diffusivity.

## 1 Introduction

The treatment of coronary artery disease using drug-eluting stents (DES) has transformed restenosis management by combining mechanical support with localized delivery of antiproliferative drugs [1]. Their effectiveness hinges on the interplay between blood flow in the lumen and drug transport into adjacent tissue, where absorption and distribution occur predominantly via diffusion [2]. Drug release and penetration are influenced by factors such as stent design, blood rheology, tissue structure, and arterial flow pulsatility [3]. Many computational models simplify these processes by treating blood as Newtonian and assuming isotropic tissue diffusion [4–7], which may limit accuracy in small-caliber arteries where stents significantly alter local hemodynamics and reduce near-wall velocities [8]. Under these conditions, non-Newtonian effects and anisotropic diffusion become critical for accurately predicting spatial drug distribution [6, 9–11].

To investigate how this flow behavior interacts with tissue transport properties, we compared square and semi-circular stent geometries under Newtonian and non-Newtonian flows, considering both isotropic and anisotropic tissue diffusivity tensors. In the anisotropic case, an axial-to-radial diffusivity ratio of 10 was adopted [5, 6, 10–12], reflecting preferential longitudinal transport along the vessel wall, which is characteristic of the healthy arterial wall where longitudinal/planar diffusivity is approximately ten times greater than radial/transmural diffusivity [5, 6, 9–12]. Incorporating this anisotropy in models significantly enhances predicted drug spread in the longitudinal direction [5, 6, 10–12]. Although many studies assume healthy tissue, stents are typically deployed in diseased vessels, where the more heterogeneous ultrastructure further complicates transport [5, 10].

To address these limitations, shear-dependent rheological models, such as Carreau or Casson, capture patient-specific shear-thinning blood behavior [3, 13], while anisotropic diffusion tensors account for direction-dependent transport influenced by tissue microstructure or flow-induced alignment [5, 6, 9–12]. These features increase

physiological realism and allow greater personalization of simulations.

In this context, we present a computational model coupling blood flow and drug transport in small-caliber arteries with DES, incorporating non-Newtonian rheology and anisotropic tissue diffusion. Blood flow in the lumen is described by the Navier–Stokes equations, tissue flow by the Brinkman equations, and drug transport by an advection–diffusion equation in the lumen coupled to anisotropic tissue diffusion. The continuous Galerkin finite element method is used with Streamline-Upwind/Petrov-Galerkin (SUPG) and Pressure-Stabilizing/Petrov-Galerkin (PSPG) stabilization to ensure numerical stability in advection-dominated flows and equal-order velocity–pressure interpolation [14–16]. Simulations compare Newtonian and non-Newtonian rheologies, with and without anisotropic diffusivity, and assess the impact of two stent geometries on hemodynamics and drug penetration, providing insights for optimizing stent design and evaluating therapeutic efficacy. These simulations provide valuable insights into optimizing stent design and enable a simulation-based assessment of therapeutic efficacy, supporting the development of improved medical devices.

## 2 Governing Equations

The mathematical model used to describe the drug-eluting stent (DES) in arterial flow is based on the steady-state incompressible flow of blood and drug diffusion within the arterial lumen and tissue. In this study, a two-dimensional representation of the left anterior descending coronary artery (LCA) was developed, assuming symmetry along the vessel's central axis and incorporating a drug-eluting stent strut. The modeled geometry corresponds to the lower half of this symmetric configuration and consists of two rectangular channels representing the lumen and the adjacent arterial tissue. These simplified configurations are consistent with idealized models commonly employed in previous studies on drug-eluting stents [3, 13]. An schematic of this domain and two stent geometries are presented in Figure 1, where the geometric dimensions were adopted according to the figure values both domain and strut.

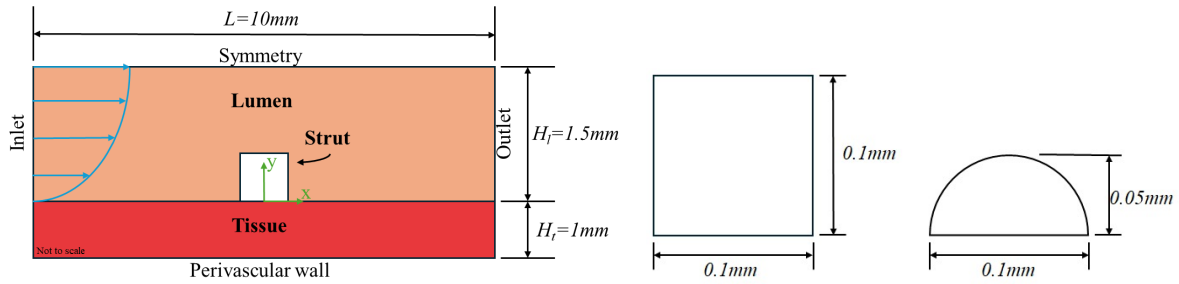



Figure 1. The computational domain with a single stent strut at the lumen-tissue interface, featuring square and semi-circular cross-sectional geometries.

The computational domain $\Omega = \Omega_l \cup \Omega_t \subset \mathbb{R}^d$ ($d = 2$ or 3) is defined by two subdomains: the lumen ($\Omega_l$), which represents the free fluid domain, and the tissue ($\Omega_t$), modeled as a porous medium. Flow in the lumen is governed by the Navier-Stokes equations, while the Brinkman equations are applied in the tissue. The boundaries are defined as $\Gamma = \Gamma_l \cup \Gamma_t$ for the lumen and tissue, and $\Gamma_s$ for the strut, with $\Gamma \cap \Gamma_s = \emptyset$. The velocities, and pressures are denoted as $\mathbf{u}^i = \mathbf{u}|_{\Omega_i}$, and $p^i = p|_{\Omega_i}$ ($i = l, t$), respectively, for the coupled problem.
*Given the viscosity $\mu$, the density $\rho$, the hydraulic conductivity $\mathbf{K}$ and the diffusivity tensors $\mathbf{D}_l$ and $\mathbf{D}_t$, find the velocity fields $\mathbf{u}^i : \Omega_i \to \mathbb{R}^d$, pressures $p^i : \Omega_i \to \mathbb{R}$ and concentration $c : \Omega \to \mathbb{R}$ (with $i = l, t$), such that*

$$\Omega_l : \begin{cases} \rho \mathbf{u}^l \cdot \nabla \mathbf{u}^l + \nabla p^l = \nabla \cdot (2\mu \mathbf{S}(\mathbf{u}^l)) \\ \nabla \cdot \mathbf{u}^l = 0 \\ -\nabla \cdot (\mathbf{D}_l \nabla c) + \mathbf{u}^l \cdot \nabla c = 0 \end{cases}, \quad \Omega_t : \begin{cases} \rho \mathbf{u}^t \cdot \nabla \mathbf{u}^t + \nabla p^t + \dfrac{\mu}{K} \mathbf{u}^t = \nabla \cdot (2\mu \mathbf{S}(\mathbf{u}^t)) \\ \nabla \cdot \mathbf{u}^t = 0 \\ -\nabla \cdot (\mathbf{D}_t \nabla c) = 0 \end{cases} \tag{1}$$

where $\mathbf{S}(\mathbf{u}) = 1/2(\nabla \mathbf{u} + \nabla \mathbf{u}^T)$. The drug diffusion in the lumen subdomain $\Omega_l$ is modeled using an isotropic diffusivity tensor $\mathbf{D}_l = D_l \mathbf{I}$, where $D_l$ is the scalar diffusion coefficient and $\mathbf{I}$ is the identity tensor. In the tissue subdomain $\Omega_t$, an anisotropic diffusivity tensor is employed, defined as $\mathbf{D}_t = \text{diag}[D_{tx}, D_{ty}]$, where $D_{tx}$ and $D_{ty}$ represent the longitudinal and transverse effective drug diffusivities, respectively. This formulation captures distinct diffusion mechanisms influenced by the tissue microstructure and flow-induced alignment, with an anisotropic ratio $D_{tx}/D_{ty} \approx 10$ based on empirical estimates [5, 6, 9–12]. The governing equations for the coupled system (1) are complemented by the boundary conditions outlined in the subsequent section.

### 2.1 Boundary conditions

Based on the domain described in Figure 1, for fluid flow in the lumen subdomain $\Omega_l$, a Poiseuille velocity profile is applied at the inlet $\Gamma_{l,in}$

$$\mathbf{u}^l|_{\Gamma_{l,in}} = u_{\max}\left(1 - \left(\frac{H_l - y}{H_l}\right)^2\right), \tag{2}$$

where $y$ is the vertical coordinate, $H_l$ is the luminal symmetry height, and $u_{\max} = 0.533\ \mathrm{m/s}$ is the maximum velocity. At the outlet $\Gamma_{l,out}$, zero-gauge pressure is imposed: $p^l|_{\Gamma_{l,out}} = 0$. No-slip conditions are enforced at the strut interface $\Gamma_s$: $\mathbf{u}^l|_{\Gamma_s} = \mathbf{u}^t|_{\Gamma_s} = \mathbf{0}$. A symmetry condition is applied at the lumen top $\Gamma_{l,top}$: $\mathbf{u}^l \cdot \mathbf{n}|_{\Gamma_{l,top}} = 0$, where $\mathbf{n}$ is the outward normal.

For drug transport, concentration is set at the strut surfaces $\Gamma_s$: $c|_{\Gamma_s} = 1$. At the inlet $\Gamma_{l,in}$, zero concentration is imposed: $c|_{\Gamma_{l,in}} = 0$. Flux continuity is enforced at the lumen-tissue interface $\Gamma_{l,t}$: $\left(-\mathbf{D}_l\nabla c \cdot \mathbf{n}\right)|_{\Gamma_{l,t}} = \left(-\mathbf{D}_t\nabla c \cdot \mathbf{n}\right)|_{\Gamma_{l,t}}$. At the perivascular wall $\Gamma_{t,periv}$, zero concentration is applied: $c|_{\Gamma_{t,periv}} = 0$. At the outlet $\Gamma_{l,out}$, zero mass flux is imposed: $\left(-\mathbf{D}_l\nabla c \cdot \mathbf{n}\right)|_{\Gamma_{l,out}} = 0$.

These conditions enable accurate simulation of coupled fluid flow and drug transport in stented arteries.

### 2.2 Blood rheology models

As appointed in [17], the simplification of blood rheology is only considered valid for flow conditions with strain rates exceeding $100\,\mathrm{s}^{-1}$, which is typical in large-caliber arteries [4] . However, the presence of the stent structure gives rise to flow regions characterized by low velocities, both proximally and distally, especially in cases involving non-aerodynamic geometries. These regions significantly influence both the drug's reabsorption by the surrounding tissue and its removal through convection by the bloodstream. As a result, lower strain rate values are commonly observed in these areas, creating conditions where non-Newtonian models become particularly relevant for accurately capturing the flow velocity profile.

To assess the influence of rheological models on the distribution of drug concentration within the tissue, four fluid types are considered: two Newtonian, with constant viscosity, and two non-Newtonian. The Newtonian types correspond to blood, with $\rho = 1060\ \mathrm{kg/m^3}$ and $\mu = 0.00345$ Pa.s and plasma, with density $\rho = 1025\ \mathrm{kg/m^3}$ and viscosity $\mu = 0.00122$ Pa.s. The non-Newtonian types represent the blood behavior through the Casson

$$\mu = 0.1\left(\sqrt{\eta} + \sqrt{\tau_y\frac{1-\exp(-100|\dot{\gamma}|)}{|\dot{\gamma}|}}\right)^2, \quad \tau_y = (0.625H)^3, \quad \eta = 0.012(1-H)^{-2.5}, \quad H = 40\% \tag{3}$$

and the Carreau

$$\mu = 0.00345 + (\mu_0 - \mu_{\infty C})\left[1 + (\lambda\dot{\gamma})^2\right]^{\frac{n_C-1}{2}}, \quad \lambda = 3.313, \quad n_C = 0.3568, \quad \mu_0 = 0.056. \tag{4}$$

viscosity models. These non-Newtonian models are shear-dependent and span the range of viscosity variations with respect to strain rate observed in clinical data [3]. At low strain rates ($\dot{\gamma} \approx 0\,\mathrm{s}^{-1}$), these models predict distinct increases in the apparent viscosity of blood, leading to significant differences among them in this regime [13]. The table 1 shows the other physical parameters used in the simulations.

Table 1. Physical parameters [3, 13]

| Parameter | Value |
|---|---|
| Hydraulic conductivity ($K$) | $1.43 \times 10^{-18}\ \mathrm{m^2}$ |
| Lumen diffusivity ($D_l$) | $3.89 \times 10^{-11}\ \mathrm{m^2/s}$ |
| Axial tissue diffusivity ($D_{tx}$) | $3.65 \times 10^{-11}\ \mathrm{m^2/s}$ |
| Transmural tissue diffusivity ($D_{ty}$) | $3.65 \times 10^{-12}\ \mathrm{m^2/s}$ |

## 3 Numerical Approach

To solve the coupled system (1), we employ a stabilized continuous Galerkin finite element method. In the lumen subdomain, the SUPG stabilization mitigates numerical oscillations due to dominant convective effects [14], while the PSPG stabilization allows equal-order interpolation for velocity and pressure fields, circumventing the inf-sup condition [15, 16]. In the tissue subdomain, only PSPG stabilization is applied due to the absence of significant convection. The nonlinear convective terms in the Navier-Stokes and Brinkman equations are linearized using a Newton–Raphson iterative scheme.

For the flow problem, let $\mathbf{u} = \{\mathbf{u}^l|_{\Omega_l}, \mathbf{u}^t|_{\Omega_t}\}$, $p = \{p^l|_{\Omega_l}, p^t|_{\Omega_t}\}$, and $\mathbf{u}^*$ denote the velocity solution from the previous Newton iteration. Defining the linearized operator $\mathcal{L}(\mathbf{u}, p) = -\nabla \cdot (2\mu\mathbf{S}(\mathbf{u})) + \rho\mathbf{u}^* \cdot \nabla\mathbf{u} + \nabla p$, the stabilized weak form is

*given $\mu$, $\rho$ and $\tau$ find* $\mathbf{u}$ *and* $p$ *in sufficiently regular function spaces, such that*

$$a(\mathbf{u}, \mathbf{v}) + c(\mathbf{u}, \mathbf{u}^*; \mathbf{v}) - b(\mathbf{v}, p) - b(\mathbf{u}, q) + s(\mathbf{u}, p; \mathbf{v}, q) = f(\mathbf{u}^*, \mathbf{u}^*; \mathbf{v}), \tag{5}$$

for all test functions $\mathbf{v}$ and $q$ in appropriate function spaces [14, 16], where

$$a(\mathbf{u}, \mathbf{v}) = \int_\Omega 2\mu\mathbf{S}(\mathbf{u}) : \mathbf{S}(\mathbf{v})\,\mathrm{d}\mathbf{x}, \qquad c(\mathbf{u}, \mathbf{u}^*; \mathbf{v}) = \int_\Omega (\mathbf{u} \cdot \nabla\mathbf{u}^* + \mathbf{u}^* \cdot \nabla\mathbf{u}) \cdot \mathbf{v}\,\mathrm{d}\mathbf{x},$$
$$b(\mathbf{u}, q) = \int_\Omega q(\nabla \cdot \mathbf{u})\,\mathrm{d}\mathbf{x}, \qquad f(\mathbf{u}^*, \mathbf{u}^*; \mathbf{v}) = \int_\Omega (\mathbf{u}^* \cdot \nabla\mathbf{u}^*) \cdot \mathbf{v}\,\mathrm{d}\mathbf{x},$$
$$s(\mathbf{u}, p; \mathbf{v}, q) = \int_{\Omega_l} \tau\mathcal{L}(\mathbf{u}^l, p^l) \cdot (\mathbf{u}^* \cdot \nabla\mathbf{v})\,\mathrm{d}\mathbf{x} + \int_\Omega \tau\mathcal{L}(\mathbf{u}, p) \cdot \nabla q\,\mathrm{d}\mathbf{x} + \int_{\Omega_t} \tau\left(\frac{\mu}{K}\mathbf{u}^t\right) \cdot \nabla q\,\mathrm{d}\mathbf{x}.$$

The system (5) is solved iteratively, updating $\mathbf{u}^*$ until the convergence criterion $\|\mathbf{u} - \mathbf{u}^*\|_0 < 10^{-10}$ is satisfied.

For the drug transport equation, once the velocity field is found, the approximation $\mathbf{u}$ is used to solve a stabilized advection-diffusion problem. Let $\mathbf{D} = \{\mathbf{D}_l|_{\Omega_l}, \mathbf{D}_t|_{\Omega_t}\}$ denote the diffusivity tensor. The weak form is

*given* $\mathbf{D}$*,* $\mathbf{u}^l$ *and* $\tau_c$ *find* $c$ *in sufficiently regular function space, such that*

$$\int_\Omega \mathbf{D}\nabla c \cdot \nabla w\,\mathrm{d}\mathbf{x} + \int_{\Omega_l} (\mathbf{u}^l \cdot \nabla c)w\,\mathrm{d}\mathbf{x} + \int_{\Omega_l} \tau_c\left(-\nabla \cdot (\mathbf{D}_l\nabla c) + \mathbf{u}^l \cdot \nabla c\right)(\mathbf{u}^l \cdot \nabla w)\,\mathrm{d}\mathbf{x} = 0, \tag{6}$$

for all test functions $w$ in an appropriate function space [14]. The stabilization coefficients adopted in this work are [16]

$$\tau = \left[\left(2\frac{\|\mathbf{u}^*\|}{h}\right)^2 + \left(4\frac{\mu}{h^2}\right)^2\right]^{-1/2} \qquad \text{and} \qquad \tau_c = \left[\left(2\frac{\|\mathbf{u}^l\|}{h}\right)^2 + \left(4\frac{\|\mathbf{D}_l\|}{h^2}\right)^2\right]^{-1/2}. \tag{7}$$

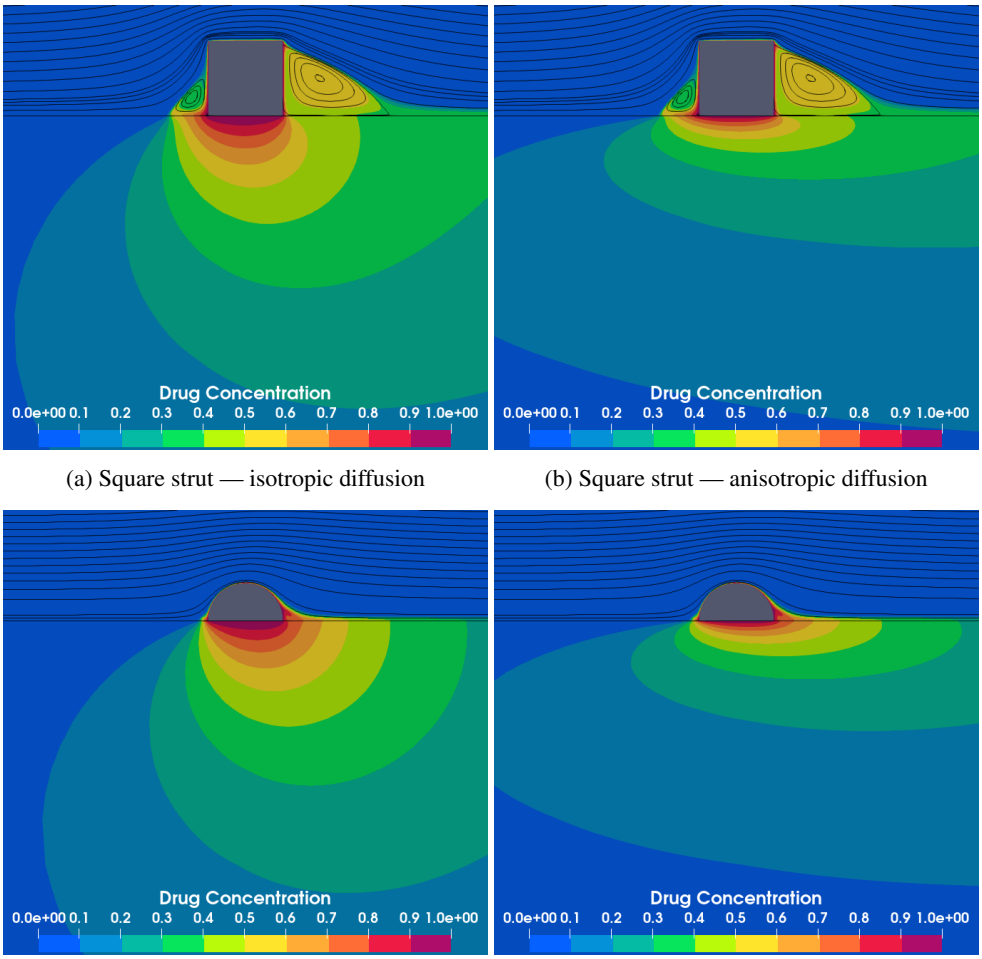
where $h$ is the minimum cell size and $\|\cdot\|$ denotes the Euclidean norm.

## 4 Results and discussion

We perform numerical simulations using the `deal.II` finite element library [18]. For our spatial discretization, we employ linear (first-order) Lagrange polynomials to represent velocity, pressure, and concentration. We simulate two strut geometries, a square and a semi-circular one, using meshes generated with targeted mesh refinement. This approach concentrates a greater number of elements in the critical region around the stent. The resulting meshes, with 197,120 elements for the square strut and 248,320 for the semi-circular, are less than one-fifth the size of those used in previous studies [3, 13], while still providing results without any loss of numerical stability or visual accuracy in the region around the stent.

### 4.1 Effects of anisotropic diffusivity tensor on spatial drug distribution

Figure 2 displays drug concentration maps under Newtonian flow, revealing that tissue diffusion anisotropy and stent geometry (square vs. semi-circular) significantly alter concentration gradients and recirculation zones, particularly in proximal and distal regions where flow separation interacts with longitudinal diffusion. For square struts, anisotropy enhances longitudinal drug spread, notably within the proximal recirculation zone, boosting accumulation, and promotes distal penetration despite flow dilution, whereas in semi-circular struts, the effect is muted due to smaller recirculation areas and greater reliance on diffusion from the strut-tissue interface. Overall, these findings highlight that anisotropic diffusion amplifies recirculation-driven drug pooling, especially in non-streamlined geometries, underscoring the need to jointly consider hemodynamic conditions and tissue microstructure for accurate drug deposition predictions.




(a) Square strut — isotropic diffusion

(b) Square strut — anisotropic diffusion

(c) Semi-circular — isotropic diffusion

(d) Semi-circular — anisotropic diffusion

Figure 2. Drug concentration distribution and flow streamlines, showcasing the effects of both strut geometry (square vs. semi-circular) and tissue diffusion (isotropic vs. anisotropic) on Newtonian blood flow.

### 4.2 Combined Effects of Rheological Models and Anisotropic Tissue Diffusivity on Drug Distribution

Figure 3 illustrates drug concentration distributions at $0.1$ mm below the luminal interface, capturing the effects of blood rheology, strut geometry (square vs. semi-circular), and tissue anisotropy on near-wall transport. Anisotropic diffusion enhances longitudinal drug spread, especially with square struts, where larger and asymmetric recirculation zones increase proximal retention and distal dispersion. However, this anisotropy also restricts vertical drug penetration, leading to higher concentration retention near the luminal surface for all combinations of geometry and rheology. Newtonian models tend to overestimate recirculation zone lengths compared to Casson and Carreau, which shifts the balance between convection and diffusion. In contrast, semi-circular struts create smaller, symmetric recirculation regions, minimizing rheological effects and producing more uniform concentration profiles across models. Still, anisotropy elongates the axial distribution near the interface, underscoring the strong influence of tissue microstructure on drug transport patterns, even under reduced hemodynamic complexity.

### 4.3 Non-Newtonian Drug Concentration Difference Factor for Anisotropic Diffusion Case

To assess the impact of blood rheology on drug distribution in the case of anisotropic diffusion, we reproduce the study developed in [3], which was conducted for the isotropic diffusion case. We use the Non-Newtonian Drug Concentration Difference ($\Delta c$), which is defined as the difference between the drug concentration for non-Newtonian blood ($c_{\mathrm{NN}}$) and for Newtonian blood ($c_{\mathrm{N}}$), given by the formula $\Delta c = c_{\mathrm{NN}} - c_{\mathrm{N}}$. Positive $\Delta c$ values indicate higher concentrations for the non-Newtonian model, and negative values indicate the opposite. This metric captures rheology-induced spatial variations in drug deposition and facilitates direct interpretation of the concentration maps.

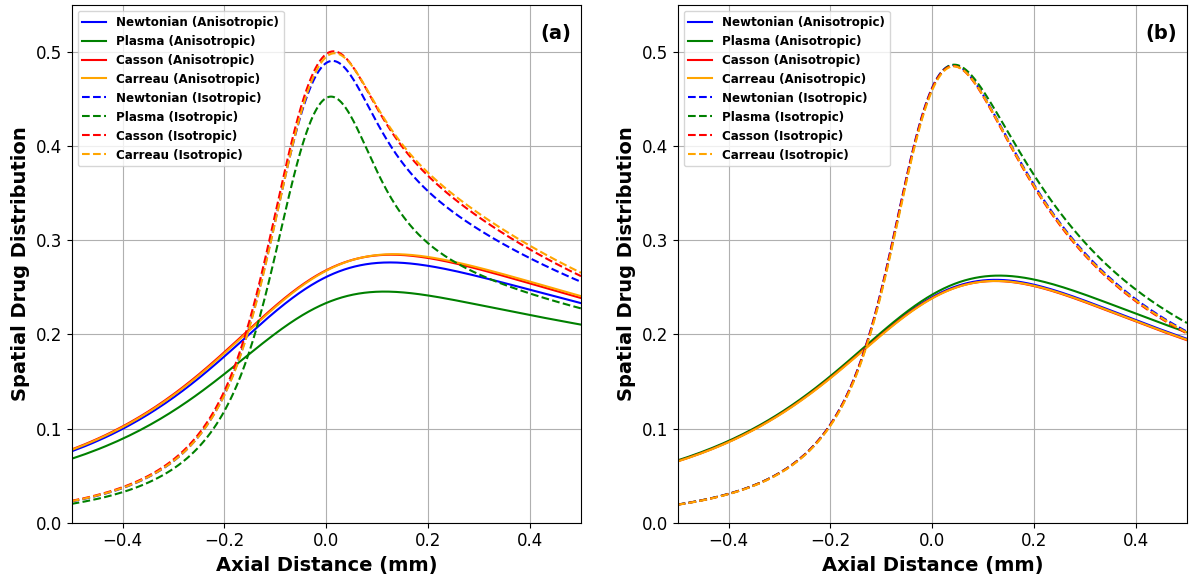



Figure 3. Spatial distribution of drug concentration at a depth of $(0.1\ \mathrm{mm})$ below the luminal interface, comparing the influences of strut geometry (square (a) vs. semi-circular (b)), blood rheology (Newtonian, Plasma, Casson, Carreau), and tissue diffusivity under isotropic ($D_{tx}/D_{ty} = 1$) and anisotropic ($D_{tx}/D_{ty} = 10$) conditions.

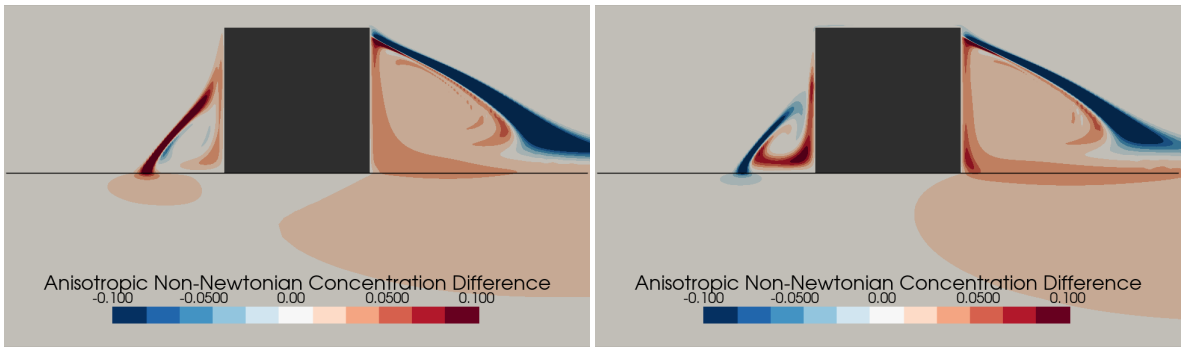



Figure 4. Contours of the anisotropic non-Newtonian drug concentration difference factor, $\Delta c$, in the square strut using (a) Casson and (b) Carreau.

As shown in Figure 4, for anisotropic tissue diffusivity, non-Newtonian models predict higher drug concentrations within both proximal and distal recirculation zones compared to the Newtonian case. In the proximal region, Casson predicts greater drug penetration into the tissue and along the outer boundary of the recirculation zone, whereas Carreau concentrates the drug along the inner perimeter of the vortex, without significant penetration into the wall. In the distal region, both models sustain higher concentrations than the Newtonian case, with Carreau producing a longer concentration zone along the lumen–tissue interface compared to Casson.

## 5 Conclusions

This study presented a unified computational framework for simulating blood flow and drug transport in small-caliber arteries with drug-eluting stents, incorporating non-Newtonian blood rheology and anisotropic tissue diffusion. The model was implemented using stabilized finite element formulations (SUPG and PSPG), ensuring accuracy in convection-dominated regimes and in the coupling between fluid and porous domains. The numerical results demonstrated that both blood rheology and tissue anisotropy have a significant impact on local drug distribution patterns. Non-Newtonian effects influenced the extent and intensity of recirculation zones, altering concentration levels proximally and distally to stent struts, while anisotropic diffusion promoted preferential longitudinal drug transport within the tissue. Furthermore, comparisons between different stent geometries revealed their influence on flow disturbances and subsequent drug penetration efficiency. These findings highlight the importance of incorporating realistic rheological and transport properties in computational models to improve predictive

capability and to support the design of more effective drug-eluting stents.

**Acknowledgements.** This work was supported by CNPq (grant number 305353/2022-5).

**Authorship statement.** The authors hereby confirm that they are the sole liable persons responsible for the authorship of this work, and that all material herein included as part of the present paper is either the property (and authorship) of the authors, or has the permission of the rightful owners to be included.

## References

[1] M. Joner, A. V. Finn, A. Farb, E. K. Mont, F. D. Kolodgie, E. Ladich, R. Kutys, K. Skorija, H. K. Gold, and R. Virmani. Pathology of drug-eluting stents in humans: delayed healing and late thrombotic risk. *Journal of the American College of Cardiology*, vol. 48, n. 1, pp. 193–202, 2006.
[2] F. Bozsak, J. M. Chomaz, and A. I. Barakat. Modeling the transport of drugs eluted from stents: physical phenomena driving drug distribution in the arterial wall. *Biomechanics and Modeling in Mechanobiology*, vol. 13, n. 2, pp. 327–347, 2014.
[3] P. R. Vijayaratnam, C. C. O'Brien, J. A. Reizes, T. J. Barber, and E. R. Edelman. The impact of blood rheology on drug transport in stented arteries: Steady simulations. *PloS One*, vol. 10, n. 6, pp. e0128178, 2015.
[4] B. Balakrishnan, A. R. Tzafriri, P. Seifert, A. Groothuis, C. Rogers, and E. R. Edelman. Strut position, blood flow, and drug deposition. *Circulation*, vol. 111, n. 22, pp. 2958–2965, 2005.
[5] B. Balakrishnan, J. Dooley, G. Kopia, and E. R. Edelman. Thrombus causes fluctuations in arterial drug delivery from intravascular stents. *Journal of Controlled Release: Official Journal of the Controlled Release Society*, vol. 131, n. 3, pp. 173–180, 2008.
[6] X. Zhu and R. D. Braatz. Modeling and analysis of drug-eluting stents with biodegradable plga coating: consequences on intravascular drug delivery. *Journal of Biomechanical Engineering*, vol. 136, n. 11, pp. 1110041–11100410, 2014.
[7] Sarifuddin and P. K. Mandal. Effect of diffusivity on the transport of drug eluted from drug-eluting stent. *International Journal of Applied and Computational Mathematics*, vol. 2, pp. 291–301, 2016.
[8] S. Tada and J. M. Tarbell. Fenestral pore size in the internal elastic lamina affects transmural flow distribution in the artery wall. *Annals of Biomedical Engineering*, vol. 29, pp. 456–466, 2001.
[9] C. W. Hwang, D. Wu, and E. R. Edelman. Physiological transport forces govern drug distribution for stent-based delivery. *Circulation*, vol. 104, n. 5, pp. 600–605, 2001.
[10] G. Vairo, M. Cioffi, R. Cottone, G. Dubini, and F. Migliavacca. Drug release from coronary eluting stents: A multidomain approach. *Journal of Biomechanics*, vol. 43, n. 8, pp. 1580–1589, 2010.
[11] W. J. Denny. *Modelling diffusion from drug eluting stents in compressed arterial tissue*. PhD thesis, University of Limerick, 2013.
[12] M. Horner, S. Joshi, V. Dhruva, S. Sett, and S. Stewart. A two-species drug delivery model is required to predict deposition from drug-eluting stents. *Cardiovascular Engineering and Technology*, vol. 1, pp. 225–234, 2010.
[13] K. Kasaeinia, R. Mohammadi, and A. Seyedhosseini. Effect of blood rheology on haemodynamics and stent-based drug delivery for coronary arteries. *European Journal of Mechanics - B/Fluids*, vol. 113, pp. 204282, 2025.
[14] A. N. Brook and T. J. R. Hughes. Streamline upwind/petrov-galerkin formulations for convection dominated flows with particular emphasis on the incompressible navier-stokes equations. *Computer Methods in Applied Mechanics and Engineering*, vol. 32, n. 1-3, pp. 199–259, 1982.
[15] T. J. Hughes, L. P. Franca, and M. Balestra. A new finite element formulation for computational fluid dynamics: V. circumventing the babuška-brezzi condition: a stable petrov-galerkin formulation of the stokes problem accommodating equal-order interpolations. *Computer Methods in Applied Mechanics and Engineering*, vol. 59, n. 1, pp. 85–99, 1986.
[16] T. Tezduyar. Stabilized finite element formulations for incompressible flow computations. *Advances in Applied Mechanics*, vol. 28, pp. 1–44, 1991.
[17] S. Berger and L.-D. Jou. Flows in stenotic vessels. *Annual Review of Fluid Mechanics - ANNU REV FLUID MECH*, vol. 32, pp. 347–382, 2000.
[18] D. Arndt, W. Bangerth, T. C. Clevenger, D. Davydov, M. Fehling, D. Garcia-Sanchez, G. Harper, T. Heister, L. Heltai, M. Kronbichler, R. M. Kynch, M. Maier, J.-P. Pelteret, B. Turcksin, and D. R. Wells. The deal.ii library, version 9.1. *Journal of Numerical Mathematics*, vol. 27, pp. 203 – 213, 2019.